TÜBİTAK

Turkish Journal of Earth Sciences

http://journals.tubitak.gov.tr/earth/

Research Article

Turkish J Earth Sci
(2022) 31: 193-207

doi:10.3906/yer-2108-17

# Mineralogical, petrological, and geochemical characteristics of Şenkaya Chrysoprase, Turkey

**H. Haluk SELİM[1,*], Aykut GÜÇTEKİN[2], Ferhan ŞAHİN[3], Mustafa KAYA[4], Beril TANÇ KAYA[4], Elanur GÜNER[5], K. Ömer TAŞ[4], Ahmet KARAKAŞ[2], Yasemin KANTARÇEKEN[6]**

[1]Department of Civil Engineering, İstanbul Gelişim University, İstanbul, Turkey
[2]Geological Engineering Department, Kocaeli University, Kocaeli, Turkey
[3]Department of Jewelry Engineering, İstanbul Commerce University, İstanbul, Turkey
[4]Geological Engineering Department, İstanbul Technical University, İstanbul, Turkey
[5]Natural Building Stones Technology, Dokuz Eylül University, İzmir, Turkey
[6]Bachelor of Arts in Jewelry Design, İstanbul Altınbaş University, İstanbul, Turkey

**Received:** 31.08.2021 • **Accepted/Published Online:** 11.02.2022 • **Final Version:** 29.03.2022

**Abstract:** Şenkaya chrysoprase is a gemstone and can be found near the Turnalı village located in the west-northwest of Şenkaya (Erzurum) county in the uplifted Kırdağ of Northeast Anatolia of Turkey. Chrysoprase only found in Şenkaya County and known with the same name commercially in Turkey is a light-dark green and cryptocrystalline structure gemstone encountered in the Örükyayla Mélange. Samples were collected from the field for defining mineralogical-petrographical, XRD, XRF, ICP-MS, optical cathodoluminescence microscopy (OCLM), FTIR-Raman and stable isotopic properties of Şenkaya chrysoprase. According to mineralogical and petrographic examination, Şenkaya chrysoprase has generally heterogeneous color distribution in macroscale and has 5 Mohs mineral hardness. Microquartz filling (10%–15%) was seen in the microexamination with serpentine as main component with partly massive opal type silica. The XRF analyses indicate that many samples had high $SiO_2$ values (91.45–94.38 wt%). As a result of trace elements, rare earth elements, Au-Pt group analyses using ICP-MS, Ni (167–387 ppm) and Co (12.57–74.78 ppm) values are quite remarkable. In the OCLM studies, few metallic minerals which could produce CL and could spread CL in different colors due to some trace activator elements were observed. Oxygen isotopic ($\delta^{18}O_{V\text{-}SMOW}$) values obtained from three chrysoprase samples are 24.8‰, 27.7‰ and 30.63‰, respectively and mean formation temperature is 96–99 °C.

**Key words:** Gemstone, ophiolitic mélange, Şenkaya chrysoprase

## 1. Introduction

Precious stones, which can be mounted on metals such as gold, silver, platinum, are widely used in the jewelry industry, where humanity is of great interest. Some of these stones evoking great interest in recent years in the jewelry industry are in Turkey (Hatipoğlu et al., 2010). A total of twenty gemstones are mined and processed in Turkey (Selim, 2015). One of them is Şenkaya chrysoprase.

Chrysoprase is a translucent and opaque type of chalcedony containing small amounts of nickel in colors ranging from light green to apple green (Figures 1a and 1b). Its worldwide occurrences are reported from USA (California, Oregon, and Arizona) and Eastern India. In Turkey, it occurs in Alaşehir (Manisa) in yellowish green, Dikmendağı area in Biga (Çanakkale) deep green, Sivrihisar (Eskişehir) in deep green (called chromium chalcedony; Lüle-Whipp, 2006), İkizce (Bursa), Turnalı villages of Şenkaya county (Erzurum). In Erzurum, due to its locality and most probably to the color, it is erroneously named as "Şenkaya emerald" (Selim et al., 2019a; Çiftçi et al., 2019). Chrysoprase is located within the Örükyayla Mélange and crystallized between serpentines and basalt levels in the typical section of the mélange.

This study includes field work and laboratory analysis aimed at determining the gemological properties of Şenkaya chrysoprase. Jewelry sector in Turkey, depending on fashion trend, uses authentic stones and exposes them for sale. Şenkaya chrysoprase gemstone is mined near the village of Turnalı located Şenkaya (Erzurum) in the Northeast Anatolia (Figure 2). Şenkaya chrysoprase, locally known by its trade name 'Şenkaya emerald', is a mineraloid of light-dark green (Vıcıl et al., 2004). The study area is located in the western part of Erzurum/Şenkaya district, within the European Datum-1950 UTM Zone

* Correspondence: hhselim@gelisim.edu.tr

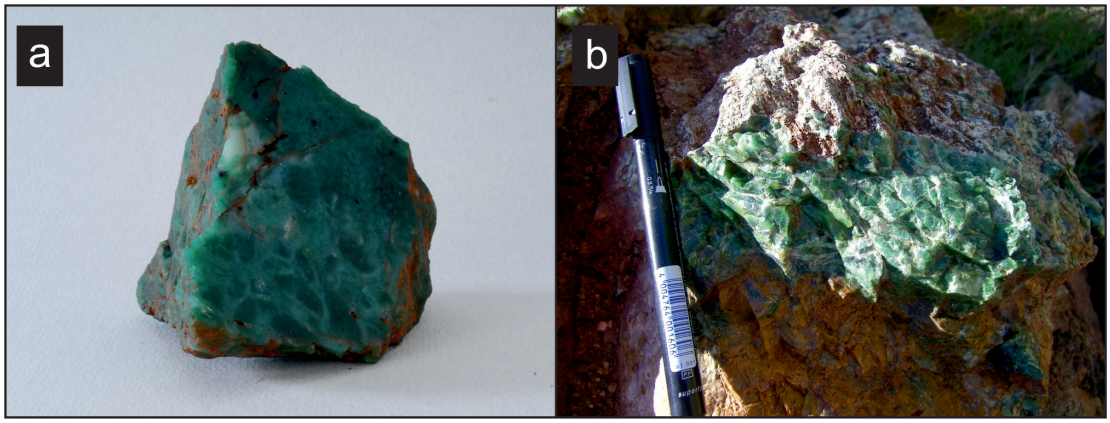


**Figure 1.** (a, b) Individual chrysoprase samples.

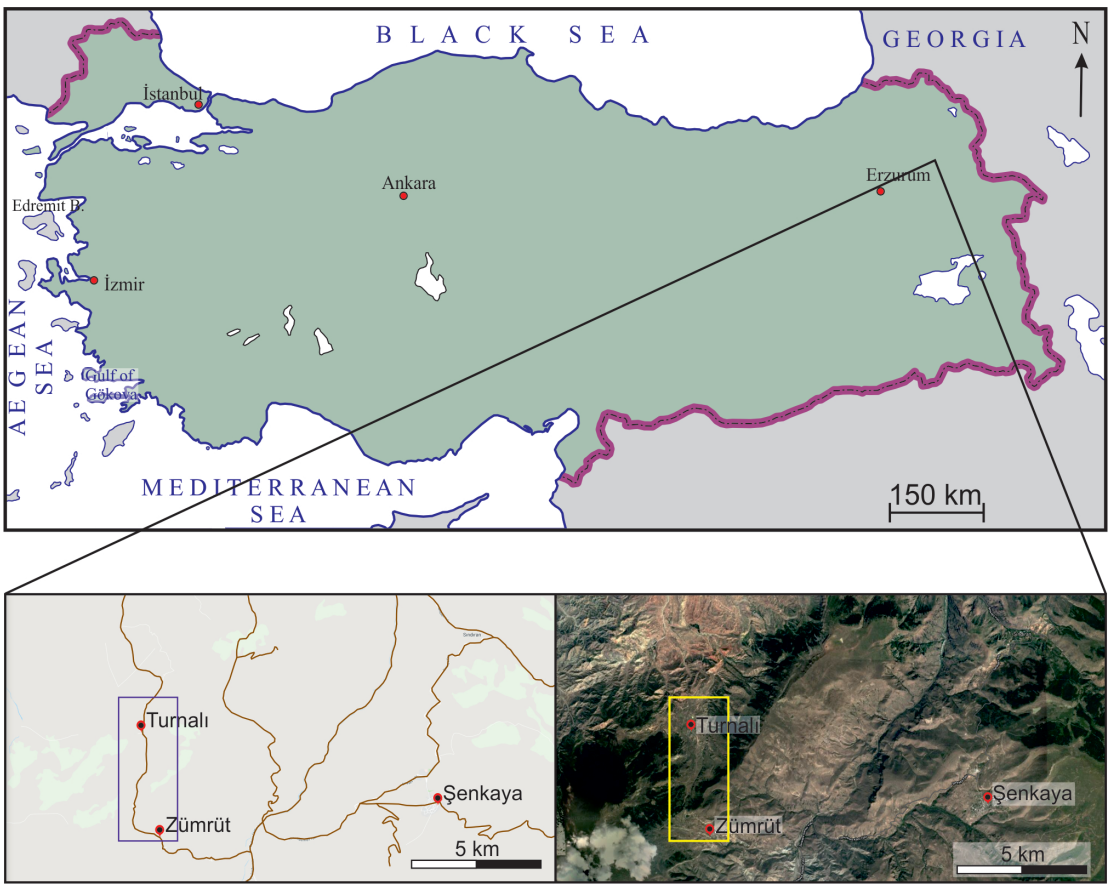


**Figure 2.** Location map of the study area.

38N 257000-4501000, 267000-4502000, 267000-4487000, 257000-4488000 corner coordinate points covered by Kars G48–d3 series K 816 in an area of about 1.5 km$^2$. Şenkaya chrysoprase has been studied in previous studies by Vıcıl et al. (2004), Konak et al. (2001), Konak and Hakyemez (2008), Zaimoğlu and Kaplanoğlu (2012), Robertson et al. (2013), Selim (2015), Şahin (2017) and Selim et al. (2019a).

Among these researchers, Vıcıl et al. (2004) have investigated the physical properties of Şenkaya chrysoprase and said that it is a mineraloid and predicted that it might be chrysoprase predominantly in field research. In addition, they stated that the water ratio in the chemical composition of the mineral constitutes 7% of the total weight. In addition, they interpreted that the mineral was a

silica gel formed below 100 °C and that this gel was formed by penetrating into the sedimentary layer cracks and crevices. Konak et al. (2001) have conducted the geological and morphological distinction of rock groups in the study area and its vicinity. In the same study, researchers named this unit, which contains green gemstones, as the "Emerald Formation".

Konak and Hakyemez (2008), by contributing to these geological studies, have defined the lithologies consisting of the sequence of rocks belonging to the Zümrüt Formation and mostly dark red colored micritic limestone, radiolarite and tectonic sliced blocks. Zaimoğlu and Kaplanoğlu (2012) have discovered that 31 types of chrysoprase are found in the Eastern Anatolia Region and that there are three types in the same location. They emphasized that these formations with emerald color and landscape patterns are the most valuable. Robertson et al. (2013) have also stated that the mineraloid is found in the formation consisting of metasandstone-shale, which is a part of the metamorphic mélange of the blueschist facies, one of the rock assemblages in the Kırdağ region. Robertson et al. (2013) have emphasized that chrysoprase was formed together with ophiolite underlying metamorphic rocks of thrust origin developed in the opposite direction in the Kırdağ region in the study area. Selim (2015) has revealed the precious and semiprecious mineral inventory in Turkey. Of these, Şenkaya chrysoprase was recorded in this inventory with a field study. Selim et al. (2019b) have also described Şenkaya chrysoprase by using the mineralogical-petrographic, geochemical and trace element methods.

This study was conducted to identify the mineralogical-petrological and geochemical properties of Şenkaya chrysoprase and to introduce the Şenkaya chrysoprase known as the trade name Şenkaya emerald and to serve a reference gemological study for semiprecious gemstones found in other parts of Turkey to contribute to the economic sector by creating awareness. This semivaluable gemstone has been processed in small-scale workshops in Erzurum and Oltu in recent years and offered for sale all over Turkey.

## 2. Geological setting

The geologic units in the study area and its surroundings are divided into two parts as basement and cover units (Figure 3). The basement units start with the Triassic Zümrüt Formation, which has undergone dynamic-metamorphism and consists of alternation of basic volcanic, volcano-clastic, and sedimentary rocks from

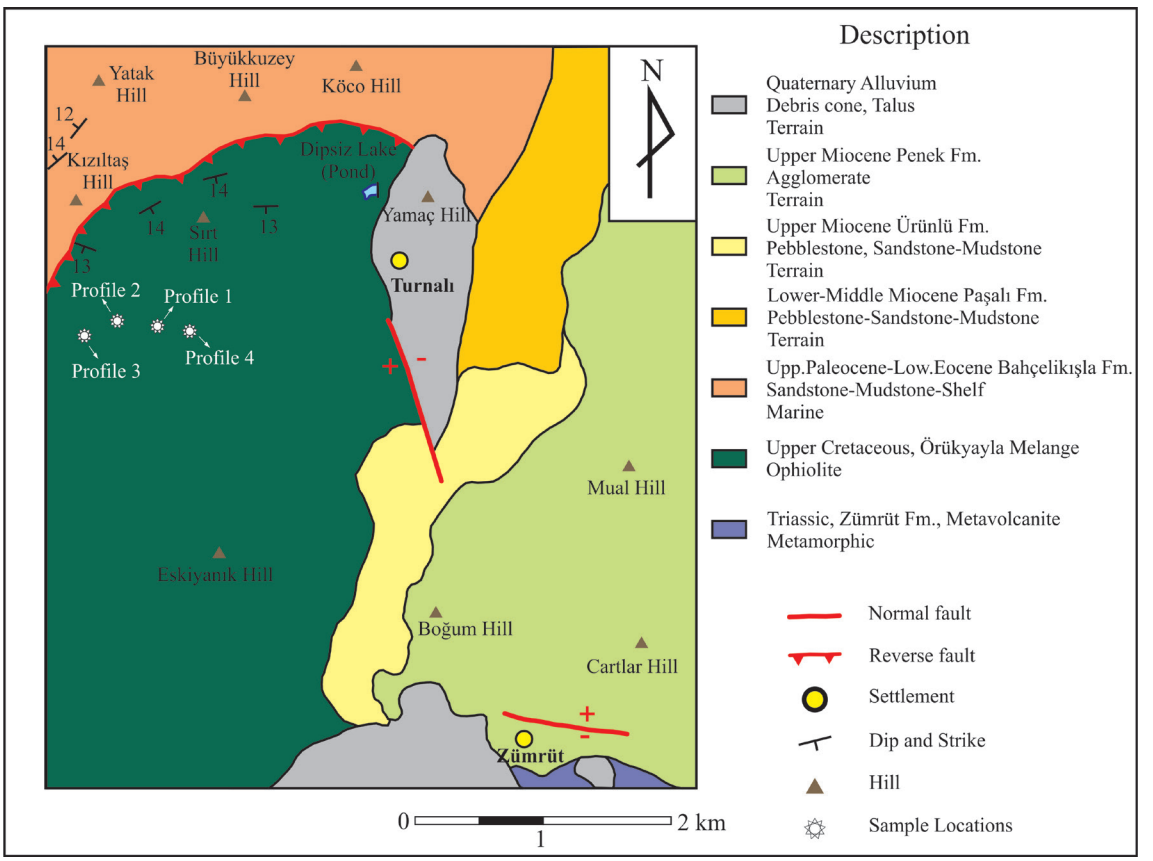


**Figure 3.** Geological map of the study area.

bottom to top. Örükyayla Mélange, which is tectonically located on the Zümrüt formation, consists of a mixture of serpentinite, gabbro, diabase, glaucophane greenschist and rocks belonging to the Zümrüt Formation, mostly dark red colored micritic limestone, radiolarite, Şenkaya chrysoprase and tectonic sliced blocks. Chrysoprase is embedded in this mélange (Figure 4). At the top of the basement units, Gedikler Ultramafic rock assemblages, which are generally composed of harzburgite, dunite and pyroxenite are encountered.

Cover units, on the other hand, begin with the Eocene Bahçelikışla Formation with a dark-layered conglomerate-sandstone alternation, colored in dark red-green, and gray from old to young. The Oligocene Toprakkale Formation, consisting of red colored mudstones with gypsum intercalation, was deposited towards the top. Later, the Late Oligocene-Early Miocene Paşalı Formation with yellow-red colored conglomerate-mudstone alternation and limestone intercalations and the Late Miocene Ürünlü Formation including the fan delta products with red colored, thick to very thick bedded and poorly sorted conglomerates, and mudstones are observed. The last of the cover units is generally black, purple, gray colored, massive or very thick layered agglomerate with sparse lava intercalations and is represented by sequences of Late Miocene Penek Formation. The youngest unit in the study area is alluvium (Konak et al., 2001).

## 3. Materials and methods

In this study, geological observations and sampling studies throughout the gemstone outcrops were carried out by the authors in two field periods covering the years 2017–2018. Approximately one hundred and fifty-two mineral and rock samples from line profiles 1–4 in Figure 5 were collected over two field periods. The first sampling campaign was carried out in season 1 along 1–2 profiles for initial assessment and then in season 2 along 3–4 profiles for detailed sampling. Samples weighing approximately six kilograms were collected for macro- and microstudies and geochemical analyses. Afterward, a sample preparation process was carried out on the bulk samples to be used in different geochemical analysis. First of all, the grain sizes of the samples were reduced to gravel size using a RETSCH BB-200 model jaw crusher. Then, samples were dried in an oven at 105 °C for 24 h. After drying process, the grain sizes of 100 g samples were reduced to <45 µm by using RETSCH (RS-200) model milling device with tungsten carbide muller. Milling process was carried out for 2 min at 1250 rpm. All dried and powdered samples were stored in a desiccator to protect from humidity.

Eighty-five thin sections from one hundred and fifty-two samples collected were prepared at the thin section laboratory of İstanbul Technical University (İTÜ). Suitable size slabs for mounting on a slide cut from appropriate rock samples taken in field studies were glued to 3 × 1.5 cm and 2 mm thick glass slides and thinned to 0.1 to 0.03 mm. Thin sections were assessed in a Leica DM4500P petrographic microscope using transmitted and reflected, plane and cross-polarized light in the Advanced Microscopy Research at İTÜ. Afterwards, thin sections analyzed under binocular microscopes provided mineralogical information about the chrysoprase and its host rock.

**Figure 4.** A field view from Şenkaya Chrysoprase in Örükyayla Mélange sequence.

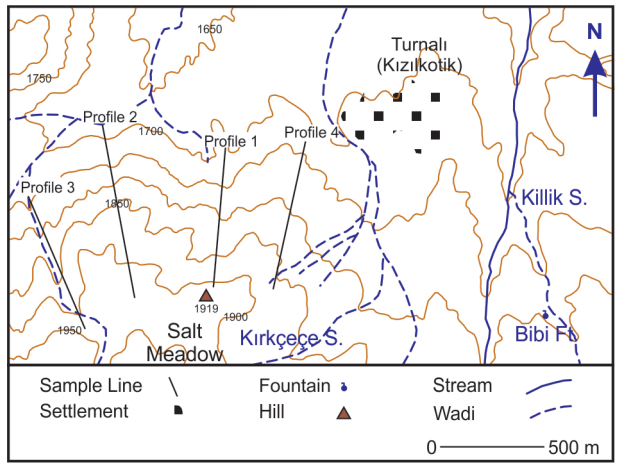


**Figure 5.** The location map where the samples of profile-1, profile-2, profile-3 and profile-4 Şenkaya chrysoprase were taken within Örükyayla Mélange in the study (Study Area Coordinates: European Datum–1950 UTM Zone N38, 262250-4497000, 264700-4497000, 264700-4495600, 2622504495600).

### 3.1. Mineral content by X-ray powder diffraction (XRPD)

X-ray powder diffraction (XRPD) analysis was used to determine mineral content of whole-rock samples to

cope with the extremely fine-grained nature of these samples. Mounted powder specimens were x-rayed in a Bruker D8 Advance X-ray diffractometer instrument with Bragg-Brentano geometry, with a Cu-tube operated at 40 kV and 40 mA producing nonmonochromated CuKα radiation of wavelength λ = 1.5406 Å. The CuKβ peak was removed with a bent graphite crystal in the diffracted beam (alternatively: by a Ni-foil in the incident beam). Diffractograms were recorded in the range of 2°–90° for each interval of 0.02°/s at room temperature and processed using DIFFRAC.EVA proprietary Bruker software, and peaks were matched against the ICDD4 database.

### 3.2. Bulk whole-rock major and trace element geochemistry

Major-minor oxides and trace elements concentrations of samples were determined in the İstanbul Technical University Geochemistry Analysis Laboratory (İTÜ-GAL) by using the BRUKER S8 TIGER model wavelength dispersive X-ray fluorescence (WDXRF) spectrometer device with 60kV/40mA power and –3/160° 2Theta geometries. Detection limit for the XRF analysis is 100 mg/kg. The milled sample and wax mixture was prepared at ratio 1:5 (w/w) and pelletized by using HERZOG model pelletizer. Loss on ignition of samples was determined by combustion approximately 2–3 g of the ground and dried samples in an ash furnace at 1050 °C for 1.5 h. In addition, CRM GSP-2 was pelletized and analyzed for the validation of XRF analysis.

Firstly, the samples were crumbled by using a jaw crusher and a hammer crusher, respectively. Then, the crumbled samples were dried in an oven at 105 °C for 24 h. After drying process, the grain sizes of 10–15 g samples were reduced to 177 μm by using RETSCH (RS-200) model milling device. Milling process was carried out for 1–2 min at 1250 rpm. All dried and powdered samples were stored in a desiccator to protect from humidity. The milled samples were pressed, pelletized then analyzed to determine major and trace elements concentration by using XRF. In the first step which all samples were decomposed; approximately 100–200 mg of milled sample was weighed to high-pressure digestion teflon vessel. Then, 8 mL of aqua regia (3:1, 37% HCl:65% $HNO_3$) and 1 mL of HF acid were added to each vessel.

PerkinElmer ELAN 6000 DRC-e model Inductively Coupled Plasma-Mass Spectrometry (ICP-MS) was used to determine trace elements including the rare earth elements (REEs) and gold-platinum group elements (PGEs) at the İstanbul Technical University Geochemistry Analysis Laboratory (İTÜ-GAL). Before the ICP-MS analysis, milled samples were completely digested in acid mixture by using BERGHOF speedwave TM MWS-3+ model microwave device. At the digestion step, 100–200 mg of milled sample was weighed to high-pressure digestion teflon vessel and 10 mL of aqua regia (3:1, HCl: $HNO_3$) and 1 mL of HF were added to each vessel. After the digestion, solution of $H_3BO_3$ 5% (w/v) was added to each vessel to remove excess of HF. Each digested sample was transferred by washing with pure water to a 50-mL volumetric flask and clear solutions of samples were obtained. Blank solution was prepared for ICP-MS analysis with the same microwave method. In addition, CRM AGV-2 was digested by the same method to validate the microwave and ICP-MS analysis method. The external standard solutions were prepared from multielement and monoelement standards (certified solutions, AccuStandard, USA).

Optical cathodoluminescence microscopy (OCLM) studies were carried out at the İstanbul Technical University Geochemistry Analysis Laboratory (İTÜ-GAL). CL, which is light or electromagnetic radiation produced by an electron beam, is an important technique that can be used for mineralogical studies in geosciences. Thus, the CL method is used to obtain information of internal textures of minerals and for the reconstruction of geological processes (e.g., Hanchar and Miller, 1993; Hanchar and Rudnick, 1995; Götze, 2000; Gorobets and Rogojine, 2002; Nasdala et al., 2004; Schertl et al., 2004; Nasdala et al., 2012). Optical cathodoluminescence microscopy (OCLM) study was carried out on uncovered polished thin sections using a CITL MK5 CL instrument mounted on a Nikon eclipse LV100 scope and integrated with an optical spectral analysis (OSA) unit and energy dispersive analysis (EDX) detector. Measurements were conducted at 15kV and 300 mA experimental conditions. High-resolution images were acquired using a low light camera and NIS software by Nikon. As a result, a formation model for the Şenkaya chrysoprase has been proposed in line with the obtained mineralogical-petrographic studies and geochemical analyses.

FTIR-Raman analyses were performed at the Ankara University Earth Sciences Application and Research Center laboratory. Raman spectra were recorded with a DILORZ24 spectrometer triple monochromator in a single channel mode, coupled to a Coherent 90-3 argon ion laser. Analyses were completed by transmitting laser at 632 nm wavelength into the sample and Raman shift spectra were obtained in the 100–1200 $cm^{-1}$ interval.

Stable isotope analyses were made on three samples in Geochron Laboratories in USA. O-H isotope analysis is the application of a method that has been widely applied for many years on many mineralization or gemstone formation due to magmatic hydrothermal solutions. The O-H isotope data of the samples were measured using thermal ionization mass spectrometry (TIMS). The precision and accuracy of isotopic measurements is 0.2‰. Oxygen is expressed relative to Vienna Standard Average Mean Ocean Water (V-SMOW); where $\delta^{18}O$ values of

SMOW are defined as zero. The methods suggested by Clayton and Mayeda (1963) and Schiffries and Rye (1989) were used on analysis procedures for stable isotope geochemistry. The definition of isotopic standards was given in detail by O'Neil (1986).

## 4. Results

### 4.1. Mineralogical-petrographic evaluation

In the study area, the best representative Şenkaya chrysoprase samples were collected along line profiles 1–4 in Figure 5. The megascopic examination and microanalysis of the samples representing each profile were performed. The macro examination of some of the specimens identified a heterogeneous color distribution varying from dark to light green hues and microcracks. Detail properties of a sample (number 2 in profile-1) representing this sample group were determined. In microanalysis, relict sieve serpentinite (45%–50%) is an example of magnesite yields (30%–35%) in the rock and cracked and lens filled secondary silica (chalcedony) formations (15%–20%). In serpentinized zones, chrysotile + antigorite mineral association is more common. Secondary magnesites were not included in a specific fracture system and were formed randomly throughout the rock. They are generally in the form of gel or cryptocrystalline magnesite. Chalcedony fillings can be lenticular with a size of approximately 3–4 mm. They show a coexistence of both random and spherulitic particles. Opaque minerals are possible chromites at a rate of 3%–4%, partially fine, generally coarse (0.5 mm) size grains. The rock is described as silicified serpentinite + magnesite (Figure 6a).

Another group of rocks has a heterogeneous color distribution ranging from dark to light green hues with a network like appearance and microcracks. Detailed properties of a sample (number 8 in profile-1) representing this sample group were determined. Macroscopically, alteration is observed as iron oxide introduction in the rock with fine to medium grain size. The microanalysis showed that the rock is composed of largely chrysotile type serpentine mineral, as well as coarse-grained crystalline magnesite in veins and lens fillings that can reach 0.5 mm in size. Serpentine mineral modal content is 65%–70%, crystalline magnesite modal content is 20%–25%. On the other hand, secondary microquartz formations are found (6%–8%), especially in magnesite walls. Opaque minerals are 1%–2% relatively coarse-grained chromites. The rock is described as serpentinite + magnesite (Figure 6b).

An important part of the specimens is green in color, brown spotted, heterogeneous in color distribution and fractured. Detailed properties of a sample (number 18c in profile-1) representing this sample group were determined. Macroscopically, alteration is observed as iron oxide introduction in the rock with fine to medium grain size. The microanalysis identified a rock consisting of 75%–80%

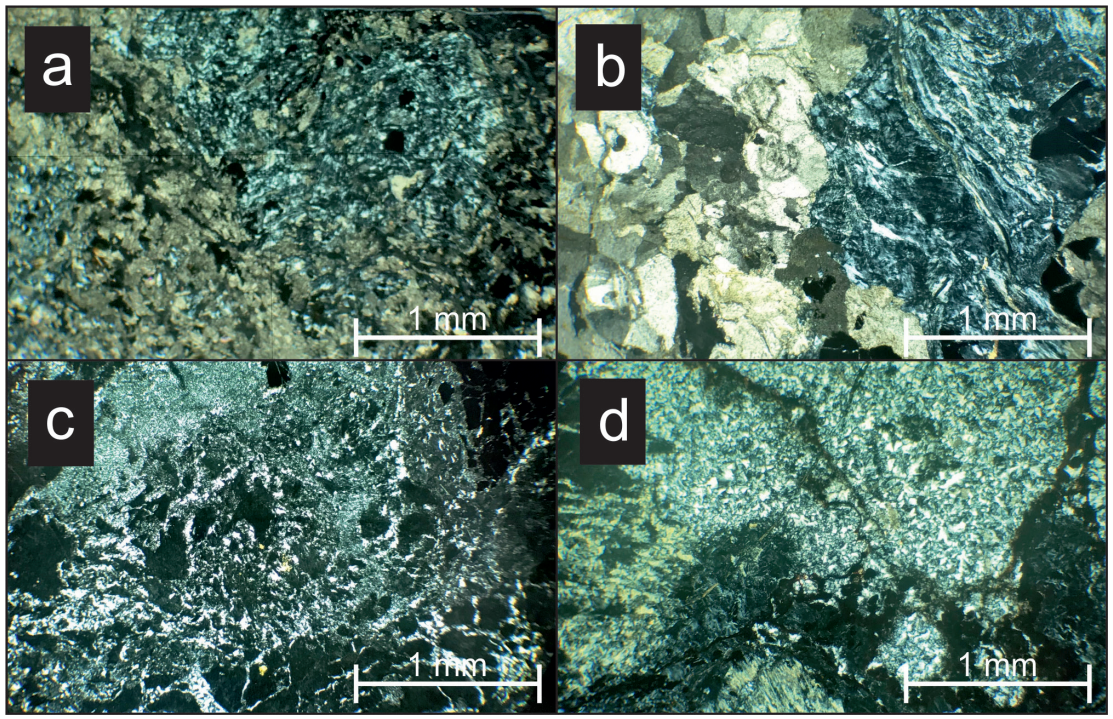


**Figure 6.** Thin section images of representative samples of a, b, c (profile-1) and d (profile-2) in the study area (all microphoto of thin section under cross-polarized light).

massive opal, as well as chalcedony and microquartz filling (10%–15%) in fine fissures and cracks as well as expanding lenses, and especially in the case of iron oxide dyed 5%–10% magnesite grains. Opaque mineral rate is 3%–4%. Although the rock is probably silicified serpentine, it does not have a serpentine-like zone and is therefore described as massive opal (Figure 6c).

The other rock group has dark green and light green color, heterogeneous color distribution and microcracks. Detailed properties of a sample (number 48 in profile-2) representing this sample group were determined. The microanalysis indicated that the rock is mainly composed of sieve textured chrysotile-antigorite type serpentine minerals (45%–50%). Secondary chalcedony formations (20%–25%) are present in the form of filling in cavities and cracks. There are massive opal transitions (10%–15%) in serpentinite zones. In general, massive opals are surrounded by magnesite shield and the ratio of this gel magnesite with very small particles together is 10%–15%. Opaque minerals are quite common in the serpentinite zone, the ratio of chromite type opaque minerals and iron oxide is 10%–15%. The rock is defined as silicified serpentinite (Figure 6d).

### 4.2. Geochemical evaluations

In this study, XRF, XRD, FTIR-Raman, $^{18}O/^{16}O$ stable isotope ratios, optical cathodoluminescence microscopy (OCLM) studies and ICP-MS analyses were carried out in order to analyze the chrysoprase samples taken in terms of formation and origin and evaluate the study area geology based on the analysis results. As a result of twelve XRF analyses performed systematically in the study area, it was observed that many samples had high $SiO_2$ values.

#### 4.2.1. X-ray powder diffractometry (XRPD)

XR**P**D analysis was applied on 12 chrysoprase samples taken from the study area. It was observed that main peaks in XR**P**D analysis consisted of cristobalites. Also, tridymite, magnesite and quartz peaks were found. Accordingly, it was determined that the Y-1 sample consisted of 50% cristobalite, 11% quartz, 27% tridymite and 12% magnesite (Figure 7). These mineral ratios are almost consistent with microscopic observations under thin section. Among the samples taken from the study area, the quartz, cristobalite and tridymite minerals, which occurred due to intense hydrothermal silica diffusion, were found in XR**P**D analysis performed on 12 samples thought to be chrysoprase. Known to be high temperature minerals, cristobalite (stable at temperatures above 1470 °C; Heaney, 1994) and tridymite (>870 °C; Kihara et al., 1986) minerals are thought to increase the quality of chrysoprase and cause a more translucent appearance.

#### 4.2.2. X-ray fluorescence spectrometer (XRF) analysis

As a result of XRF analysis, it was determined that many samples have very high $SiO_2$ (91.45%–94.38%) values.

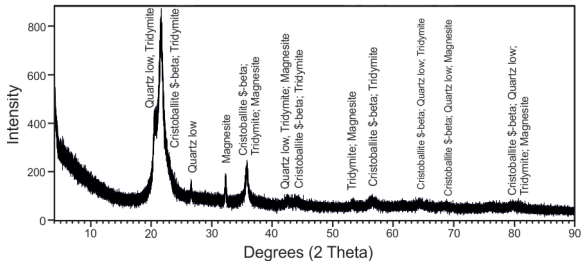


**Figure 7.** Results of XRD analysis of Şenkaya chrysoprase, selected Y-1 sample from profile-1.

The amount of Ni in some samples gives an anomaly. Al, Fe and Mg amounts are very low. When looking at the evaluations of XRF major oxide analysis performed on 12 selected samples, it was observed that the lowest $SiO_2$ amount was 91.45% and the MgO amount was 48%. It was determined that the $SiO_2$ amounts of other samples in the area in the southern region and in the zone close to dacitic volcanism were observed to have the highest $SiO_2$ amounts at 94.38%, and the MgO amount to be lower at 22%, and chrysoprase was more settled in this zone. This result shows that samples with high MgO content are typical magnesite samples, and these samples are observed in serpentine formations (Table 1).

#### 4.2.3. ICP-MS analysis

ICP-MS analysis was used to determine trace elements, rare earth elements (REEs), gold and platinum group elements (PGEs). When the trace element, rare earth element and Au-Pt group analyses performed on the samples with the ICP-MS method, Ni and Co values stand out. The trace element contents of the samples reveal enrichments in LIL elements such as Ba, Sr and HFS elements such as U and Y (Table 2). The low concentration HFS elements in these samples indicate the possibility of the highly acidic nature of the hydrothermal fluid interacting with the host rock.

#### 4.2.4. Optical cathodoluminescence microscopy (OCLM) studies

OCLM is a special type of emission of photons whose wavelengths change from ultraviolet to infrared due to being excited from a certain source (e.g., from an electron gun). The main emission event involves an electron transition from an excited state (Ee) to the normal state (Eg) with a lower energy level. OCLM or photon emission is usually intrinsic or extrinsic. Intrinsic OCLM centers are associated with band-to-band electron and hole pair recombination. Intrinsic OCLM propagation may also be associated with lattice defects (anion gap). This type of OCLM is also called defect "OCLM centers". Other intrinsic OCLM propagations are those associated with radiation and those associated with electron defects on broken bonds (Götze, 2002) (Figures 8a–8c).

**Table 1.** Main element oxide contents in whole-rock Şenkaya chrysoprase from profile-1 and profile-2, in weight percent (%), by XRF (DL: detection limits).

| Sample no | T2-1 | T2-16 | T2-18a | T2-18c | T2-19a | T2-20 | T2-26a | T2-37 | T2-46 | T2-55 | T2-78 | T2-80 | DL |
|---|---|---|---|---|---|---|---|---|---|---|---|---|---|
| **$SiO_2$** | **93.25** | **93.41** | **94.02** | **94.04** | **93.42** | **92.65** | **93.20** | **93.34** | **92.44** | **91.45** | **92.21** | **94.38** | 0.01 |
| $Al_2O_3$ | 1.49 | 0.72 | 0.32 | 0.27 | 0.26 | 0.76 | 0.30 | 0.64 | 0.73 | 1.43 | 0.71 | 0.61 | 0.01 |
| $Fe_2O_3$ | 0.79 | 1.93 | 1.23 | 1.64 | 2.63 | 2.16 | 2.91 | 2.36 | 1.53 | 1.66 | 2.08 | 1.28 | 0.01 |
| MgO | 0.40 | 0.45 | 0.13 | 0.20 | 0.25 | 0.37 | 0.15 | 0.26 | 0.23 | 0.48 | 0.28 | 0.22 | 0.01 |
| CaO | 0.39 | 0.17 | 0.06 | 0.09 | 0.42 | 0.34 | 0.05 | 0.13 | 0.15 | 0.18 | 0.17 | 0.14 | 0.01 |
| $Na_2O$ | 0.15 | 0.08 | 0.12 | 0.11 | 0.03 | 0.08 | 0.07 | 0.09 | 0.14 | 0.13 | 0.09 | 0.09 | 0.01 |
| $K_2O$ | 0.31 | 0.10 | 0.03 | 0.03 | 0.04 | 0.08 | 0.05 | 0.07 | 0.07 | 0.14 | 0.08 | 0.05 | 0.01 |
| $TiO_2$ | 0.08 | 0.01 | 0.01 | - | - | - | - | - | 0.01 | 0.01 | - | 0.01 | 0.01 |
| MnO | 0.00 | 0.01 | - | 0.01 | 0.05 | 0.02 | 0.04 | - | 0.02 | 0.02 | 0.01 | - | 0.01 |
| $Cr_2O_3$ | 0.43 | 0.42 | 0.42 | 0.33 | 0.41 | 0.41 | 0.39 | 0.41 | 0.81 | 0.78 | 0.41 | 0.43 | 0.01 |
| Cl | 0.08 | 0.03 | 0.04 | 0.05 | 0.01 | 0.02 | 0.04 | 0.02 | 0.03 | 0.02 | - | 0.01 | 0.01 |
| Ni | - | - | - | - | - | 0.07 | - | - | - | 0.05 | - | - | 0.01 |
| $SO_3$ | 0.07 | 0.07 | - | - | - | 0.03 | 0.02 | 0.02 | 0.02 | - | 0.02 | 0.02 | 0.01 |
| LOI | 2.5 | 2.53 | 3.56 | 3.16 | 2.37 | 2.96 | 2.71 | 2.58 | 3.71 | 3.60 | 3.86 | 2.68 | |
| TOTAL | 99.94 | 99.92 | 99.95 | 99.95 | 99.89 | 99.95 | 99.93 | 99.92 | 99.89 | 99.96 | 99.92 | 99.92 | |

#### 4.2.5. FTIR-Raman spectroscopy

FTIR-Raman analyses were conducted in the Ankara University Earth Sciences Application and Research Center laboratory on the eighteen selected samples taken from the profile-1, profile-2 and profile-3 sampling lines in the study area. Fourier transformed infrared (FTIR-Raman) and diffuse visible region confocal micro-Raman (DVCμR) spectroscopic graphs according to X-ray diffraction data using comparative matching technique obtained from Şenkaya chrysoprase samples approved the cryptocrystalline and crystalline-silica formation phases (Figures 9a and 9b).

The dispersive confocal micro-Raman (DClR) spectrum of a representative chrysoprase sample in the range between 300 and 800 $cm^{-1}$ was given in Figure 9a. These phases are proportional to the increase in the cooling temperature of the chrysoprase material from the edge wall towards the center. However, in the spectroscopic data obtained, opal-quartz silica forming phases (opal-CT and opal-C) are found a little in these chrysoprase samples.

#### 4.2.6. Stable isotope analysis ($\delta^{18}O_{V\text{-}SMOW}$)

The $^{18}O/^{16}O$ isotope analysis approach is a method used to reveal the temperature conditions under which the chrysoprase crystallized or the temperature records. It is based on precise measurement of the ratio between the two isotopes of oxygen in the mineral. These isotopes are $^{16}O$ being the most common and $^{18}O$ isotope heavier than $^{16}O$ isotope. The $^{18}O/^{16}O$ ratio determines the crystallization temperature range and physico-chemical formation conditions of chrysoprase. It turns out that the Şenkaya chrysoprase deposited under formation temperature conditions, relatively higher than 55 °C, possibly in the range of 60–130 °C. In order to further specify this temperature range value by using the oxygen isotope fractionation in the chrysoprase-water formation system, the oxygen isotopic ($\delta^{18}O_{V\text{-}SMOW}$) values obtained from three different Şenkaya chrysoprase samples are +24.8‰ (for T2-3 sample), +27.7‰ (for T2-51 sample) and +30.63‰ (for T2-54 sample), respectively (Table 3).

## 5. Usage of chrysoprase in the jewelry industry

Cutting and processing techniques are applied by using various machines in the jewelry sector. These techniques are facet cutting, cabochon cutting, carving techniques (cameo, intaglio), ball (bead), slice cutting, and decorative ornament object applications. Şenkaya chrysoprase is generally handled in cabochon forms in the region where it is located, and its upper part is flat under camber (Şahin, 2017; Şahin et al., 2017). Cabochon cutting is a technique of processing all kinds of geometric and amorphous patterns made to ornamental stones with a flat lower part and a curved upper part with or without a facet. The facet cutting technique, on the other hand, is the cutting process performed at certain angles and sizes with various diagrams applied to gemstones and precious stones. There are quite a lot of fancy cut models that can be applied to

**Table 2.** Trace element, REE, and PGM contents in whole-rock Şenkaya chrysoprase from profile-1 and profile-2, in parts per million (ppm; μg $g^{-1}$), by ICP-MS (DL: detection limits; ND: not detected).

| Sample No | T2-1 (ppm) | T2-16 (ppm) | T2-18a (ppm) | T2-18c (ppm) | T2-19a (ppm) | T2-20 (ppm) | T2-26a (ppm) | T2-37 (ppm) | T2-46 (ppm) | T2-55 (ppm) | T2-78 (ppm) | T2-80 (ppm) | DL (ppb) |
|---|---|---|---|---|---|---|---|---|---|---|---|---|---|
| Sc | 86.66 | 100.74 | 96.75 | 91.97 | 92.71 | 93.15 | 94.80 | 93.31 | 103.26 | 97.90 | 89.97 | 91.39 | 0.001 |
| Y | 0.29 | 0.28 | 0.25 | 0.22 | 0.98 | 0.80 | 0.71 | 2.07 | 1.25 | 22.78 | 0.21 | 0.55 | 0.00002 |
| La | 0.29 | 0.27 | 0.08 | 0.14 | 0.26 | 0.32 | 0.40 | 1.51 | 0.28 | 3.69 | 0.11 | 0.28 | 0.00004 |
| Ce | 0.47 | 0.42 | 0.14 | 0.19 | 0.31 | 0.33 | 0.38 | 2.73 | 0.57 | 0.39 | 0.16 | 0.53 | 0.00005 |
| Pr | 0.07 | 0.06 | 0.02 | 0.03 | 0.09 | 0.08 | 0.10 | 0.32 | 0.07 | 1.28 | 0.00 | 0.05 | 0.00003 |
| Nd | 0.25 | 0.25 | 0.12 | 0.16 | 0.45 | 0.36 | 0.58 | 1.47 | 0.28 | 6.54 | 0.12 | 0.36 | 0.0003 |
| Sm | 0.09 | 0.05 | 0.03 | 0.04 | 0.11 | 0.09 | 0.13 | 0.27 | 0.08 | 1.90 | 0.01 | 0.06 | 0.0002 |
| Eu | 0.04 | 0.03 | 0.01 | 0.02 | 0.03 | 0.02 | 0.05 | 0.06 | 0.03 | 0.61 | ND | ND | 0.00007 |
| Gd | 0.07 | 0.05 | 0.03 | 0.03 | 0.15 | 0.09 | 0.14 | 0.34 | 0.09 | 2.86 | 0.01 | 0.06 | 0.0003 |
| Tb | 0.01 | 0.00 | 0.00 | 0.00 | 0.02 | 0.01 | 0.02 | 0.01 | 0.02 | 0.51 | ND | ND | 0.00003 |
| Dy | 0.05 | 0.02 | 0.03 | 0.03 | 0.15 | 0.08 | 0.08 | 0.23 | 0.13 | 3.74 | ND | 0.06 | 0.0002 |
| Ho | 0.02 | 0.01 | 0.00 | 0.01 | 0.03 | 0.02 | 0.02 | 0.02 | 0.03 | 0.78 | ND | ND | 0.00004 |
| Er | 0.03 | 0.02 | 0.02 | 0.02 | 0.11 | 0.07 | 0.07 | 0.16 | 0.13 | 2.36 | ND | 0.02 | 0.0001 |
| Tm | 0.01 | 0.01 | 0.00 | 0.00 | 0.02 | 0.01 | 0.01 | ND | 0.02 | 0.27 | ND | ND | 0.00003 |
| Yb | 0.04 | 0.02 | 0.01 | 0.01 | 0.13 | 0.05 | 0.06 | 0.15 | 0.12 | 1.78 | ND | 0.00 | 0.0001 |
| Lu | 0.01 | 0.00 | 0.00 | 0.00 | 0.02 | 0.01 | 0.01 | ND | 0.02 | 0.21 | ND | ND | 0.00004 |
| Th | 0.16 | 0.06 | 0.01 | 0.05 | 0.02 | 0.03 | 0.03 | ND | 0.05 | ND | ND | ND | 0.00005 |
| Li | 2.21 | 3.75 | 1.84 | 2.73 | 5.25 | 2.62 | 2.25 | 1.39 | 3.37 | 1.62 | 1.52 | 1.11 | 0.00005 |
| Be | 0.75 | 0.51 | 0.49 | 1.13 | 0.05 | 0.94 | 1.55 | 0.62 | 1.42 | 0.81 | 0.36 | 0.52 | 0.0003 |
| **Co** | **22.04** | **28.99** | **12.57** | **15.71** | **39.43** | **31.42** | **22.22** | **26.65** | **74.78** | **20.20** | **31.31** | **25.07** | 0.00006 |
| **Ni** | **167.88** | **361.83** | **166.92** | **206.97** | **387.07** | **HC** | **263.16** | **317.22** | **223.33** | **HC** | **363.56** | **257.87** | 0.0002 |
| Cu | 28.24 | 8.33 | 1.82 | 2.49 | 10.83 | 9.52 | 25.36 | 25.22 | 10.01 | 42.18 | 18.36 | 22.82 | 0.0002 |
| Zn | 28.52 | 6.08 | 17.75 | 16.22 | 14.68 | 23.18 | 12.54 | 7.65 | 20.24 | 21.89 | 17.85 | 109.96 | 0.0007 |
| Ga | 2.85 | 0.83 | 0.23 | 0.31 | ND | 0.72 | 0.49 | 1.24 | 1.13 | 2.30 | 0.29 | 0.25 | 0.00008 |
| As | 56.74 | 69.56 | 50.61 | 50.27 | 35.87 | 93.30 | 42.74 | 122.37 | 28.69 | 122.64 | 133.95 | 114.23 | 0.0004 |
| Se | ND | ND | ND | ND | ND | ND | ND | ND | ND | ND | ND | ND | 0.0003 |
| Rb | 4.09 | 2.18 | 1.12 | 1.02 | 0.72 | 1.88 | 0.95 | 2.31 | 1.77 | 5.76 | 2.80 | 2.32 | 0.0002 |
| Sr | 16.82 | 14.68 | 9.63 | 9.25 | 8.38 | 14.67 | 6.66 | 8.93 | 10.95 | 15.22 | 11.49 | 11.12 | 0.00007 |
| Ag | 0.18 | ND | ND | 0.03 | ND | 0.00 | 0.01 | 0.16 | 0.03 | 0.31 | 0.07 | 0.08 | 0.00009 |
| Cd | 0.00 | 0.03 | 0.04 | 0.03 | 0.03 | ND | ND | 0.05 | 0.00 | ND | ND | 0.03 | 0,00007 |
| In | 0.02 | ND | ND | 0.01 | 0.00 | 0.00 | ND | ND | ND | ND | ND | ND | 0.00008 |
| Cs | 0.41 | 0.55 | 0.19 | 0.17 | 0.11 | 0.52 | 0.16 | 0.51 | 0.40 | 2.26 | 0.93 | 0.57 | 0.00005 |
| Ba | 64.50 | 40.84 | 15.06 | 17.04 | 11.84 | 35.80 | 26.80 | 33.59 | 29.36 | 47.64 | 25.99 | 31.16 | 0.00004 |
| Tl | 0.10 | 0.03 | 0.01 | 0.00 | 0.00 | 0.04 | 0.02 | 0.02 | 0.06 | 0.14 | 0.03 | 0.05 | 0.00001 |
| Pb | 2.05 | 1.50 | 2.40 | 2.23 | 1.75 | 1.79 | 0.15 | 3.09 | 1.40 | 1.81 | 2.22 | 3.87 | 0.00004 |
| U | 0.05 | 0.25 | 0.04 | 0.06 | 0.02 | 0.24 | 0.17 | 0.34 | 0.04 | 0.18 | 0.08 | 0.14 | 0.00002 |
| Au | 0.09 | 0.01 | 0.01 | 0.02 | 0.01 | 0.01 | 0.01 | 0.02 | 0.01 | 0.02 | ND | ND | 0.0001 |
| Hf | 0.17 | 0.05 | 0.04 | 0.03 | 0.00 | 0.05 | 0.03 | 0.05 | ND | 0.05 | ND | ND | 0.0003 |
| Ir | 0.01 | 0.00 | 0.00 | 0.00 | 0.01 | 0.00 | ND | 0.02 | 0.00 | 0.02 | ND | ND | 0.00009 |

**Table 2.** (Continued).

| | | | | | | | | | | | | | |
|---|---|---|---|---|---|---|---|---|---|---|---|---|---|
| Pd | 0.07 | 0.05 | 0.06 | 0.06 | 0.06 | 0.06 | 0.05 | 0.15 | 0.05 | 0.21 | 0.15 | 0.14 | 0.00003 |
| Pt | 0.01 | 0.01 | 0.01 | 0.01 | 0.01 | 0.01 | 0.01 | 0.02 | 0.02 | 0.05 | ND | ND | 0.0001 |
| Rh | 0.00 | ND | 0.00 | 0.00 | ND | ND | ND | 0.01 | ND | 0.02 | 0.01 | ND | 0.00004 |
| Ru | 0.02 | 0.05 | 0.06 | 0.05 | 0.03 | 0.04 | 0.04 | 0.08 | 0.05 | 0.08 | 0.07 | 0.08 | 0.0001 |
| Sb | 0.40 | 0.52 | 0.45 | 0.62 | 0.39 | 0.80 | 0.36 | 0.40 | 0.30 | 0.37 | 0.31 | 0.28 | 0.0002 |
| Sn | 1.49 | 0.69 | 1.09 | 0.79 | 1.37 | 0.71 | 0.84 | 0.93 | 0.90 | 0.99 | 0.68 | 0.56 | 0.0002 |

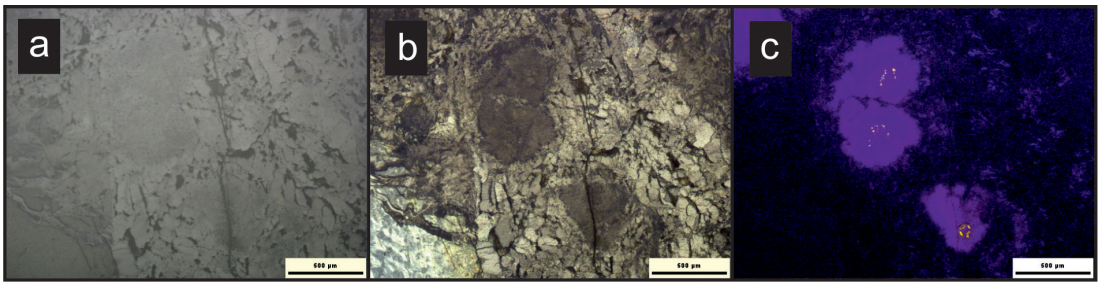


**Figure 8.** (a, b, c) Images of optical cathodoluminescence microscopy (OCLM) analysis of Şenkaya chrysoprase, selected 59 sample from profile-3.

stones other than the facet cut, diamond cut, princess cut, emerald cut applied in the sector. Today, facet (geometric shape cutting) cutting has developed so much that, due to laser technology, very special drill bits, geometric shapes are cut and polished with a sensitivity of less than 1 mm. Carving techniques are the process of carving formed precious and semiprecious stones with diamond tools. Cameo technique is the process of embossing the motif positively (outward) by using oil, water and various polishing powders on ornamental stones, diamond bits and hand milling. The Intaglio technique is the process of carving the motif in a negative direction (inward) on precious or semiprecious stones, using oil, water, and various polishing powders, by using diamond bits and hand milling. Şenkaya chrysoprase is extracted by the local people, processed in workshops in Oltu (Erzurum) and sold by more than sixty tradesmen (Figure 10).

## 6. Discussion

Chrysoprase is economically available in certain countries in the world such as Poland, Kazakhstan, Australia, Brazil, Tanzania, and Turkey. The important chrysoprase deposits providing quality stone for jewelry in Turkey are located in Biga (Çanakkale), Sivrihisar (Eskişehir), Savur (Mardin), İkizce (Bilecik) and in the study area of Şenkaya (Erzurum) (Hatipoğlu et al., 2016). It is important that chrysoprase is particularly rich in cobalt (Co) and nickel (Ni), surrounded by a weathered crust at the contact of the serpentinites and found as crack fillings.

Petrographic studies reveal that the mineralogical inner structural feature (silica formation phases) of Şenkaya chrysoprase consists of three phases: chalcedony-quartz, moganitic-quartz, and alpha-quartz. The first of these, chalcedony phase (cryptocrystalline chalcedonic silica formation phase) is mostly composed of radial thread structure [long axis damped chalcedony] and a small amount is composed of fine-grained (length-slow chalcedony or lutecite) silica formation matrices. The original description of lutecite has given by Michel-Levy and Munier-Chalmas (1892). Heaney and Post (1992) have identified lutecite as identical with moganite and defined it same as 'length-slow chalcedony'. Secondly, the moganite phase-cryptocrystalline moganite silica formation phase consists entirely of coarse grained (short axis damped moganite) silica formation matrix. Moganite, a polymorph of quartz, crystallizes in the monoclinic system. Third, the alpha-quartz phase-crystalline alpha-quartz silica formation phase (generally in the form of macroscopic quartz crystals in the form of the latest cooling inclusion in the center of the material) coarse crystalline silica (alpha-quartz) consists of inclusions as a silica formation matrix.

The descriptions of these microscopic silica-forming phases are based on X-ray diffraction data (Table 1) using Fourier transformed infrared (FTIR) (see Figure 9a) and scattered visible region confocal microdata using comparative matching technique. According to Raman (DVCμR) spectroscopic graphs (see Figure 9b), it also appears as cryptocrystalline and crystalline-silica formation phases. These phases are proportional to the increase in the cooling temperature of the chrysoprase material from the edge wall towards the center. However, in the spectroscopic data obtained, opaline-quartz silica

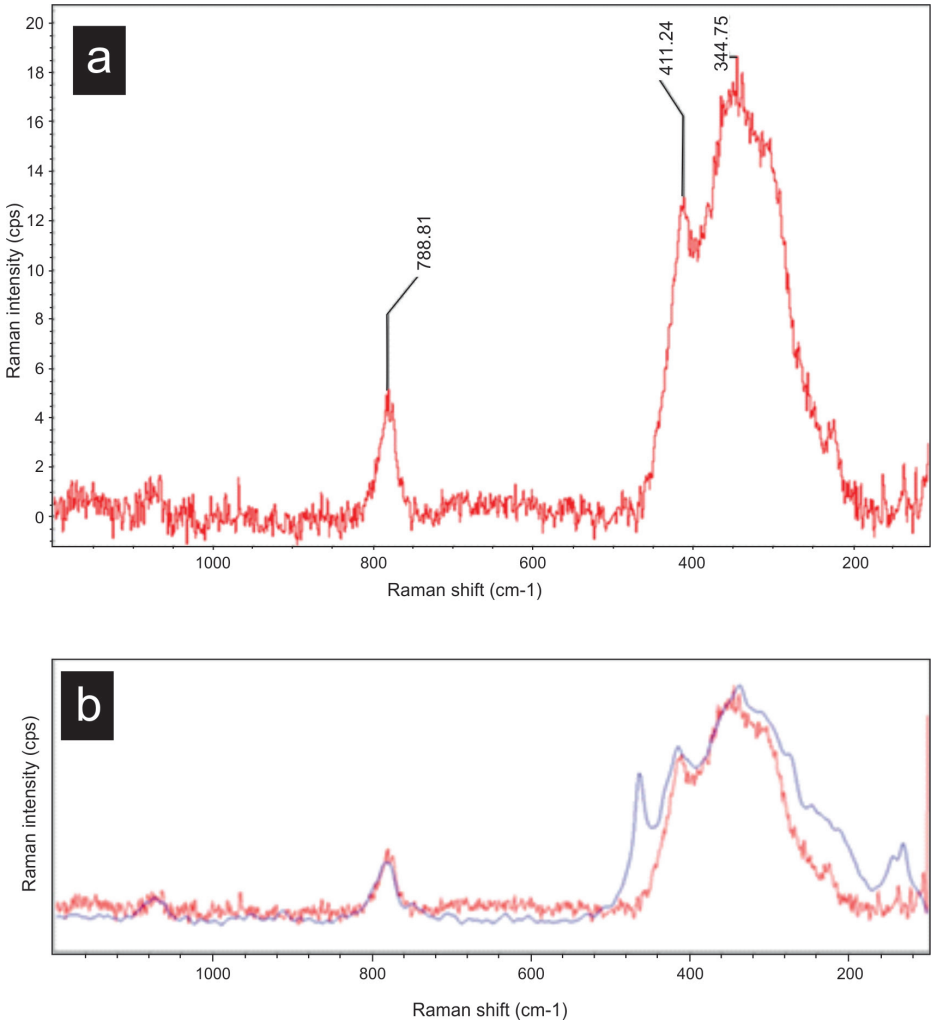


**Figure 9.** (a) Fourier transform infrared FTIR spectroscopic image of the selected 26B sample from profile-1. (b) Fourier transform infrared Raman spectroscopic composite image of selected 26B sample from profile-1. In this sample, Opal CT ($SiO_2.nH_2O$) mineral is seen prominently in (green) 781.88, 411.24 and 344.75 $cm^{-1}$ peaks.

forming phases (opal-CT and opal-C) could not be found in these chrysoprase samples. As a result, it is revealed that the silica formation phases of Şenkaya chrysoprase samples are relatively homogeneous. It can be said that the chalcedonic-quartz silica formation phase is approximately 95%, and the moganite and alpha-quartz silica formation phases are approximately 5%.

On the other hand, Şenkaya chrysoprase due to a) the presence of chalcedonic and moganite-quartz silica formation phases (chalcedony and moganite) instead of opaline-quartz silica base phases (opal-CT and opal-C), b) the homogeneous temperature values obtained from fluid inclusions, relatively higher than 55 °C appear to have been deposited at formation temperature conditions, possibly in the range of 60–130 °C. In order to further constrain this temperature range using the oxygen isotope

**Table 3.** Results of stable isotope analysis ($\delta^{18}O_{V\text{-}SMOW}$) of Şenkaya chrysoprase.

| Sample number | Sample description | $\delta^{18}O$ |
|---|---|---|
| T2-3 (Profile-1) | Rock powder | +27.7 |
| T2-51 (Profile-3) | Rock powder | +24.8 |
| T2-54 (Profile-3) | Rock powder | +30.63 |

fractionation in the chrysoprase-water formation system, oxygen stable isotope ($\delta^{18}O_{V\text{-}SMOW}$) values taken from three different Şenkaya chrysoprase samples were obtained as 24.8‰, 27.7‰ and 30.63‰ with a mean 28.38‰. These positive high oxygen isotope values indicate the presence of meteoric water ($\delta^{18}O_{V\text{-}SMOW}$= +4‰). It is accepted in the

**Figure 10.** Facet cutting and carving techniques and usage of Şenkaya chrysoprase in jewelry industry, Oltu (Erzurum).

calculations that the $\delta^{18}O$ value of water present during formation of chrysoprase, was not lower than –8‰ but not higher than 4‰ (Skrzypek et al., 2003a). Although, the general formation mechanism and depositional conditions of chrysoprases vary according to the colloidal form of silicic acid ($H_4SiO_4$) circulating in cracks and spaces, pH (alkaline, 8-9) and Eh (e.g., ambient temperature, origin of water (meteoric or magmatic), water-rock ratio) characteristics, the positive high oxygen isotope values of Şenkaya chrysoprase, which clearly indicate the presence of meteoric water, are consistent with both the geological formation positions of these chrysoprases and the mineralogically silica formation phases (chalcedonic- and moganite-quartz phases).

In addition, serpentinites are the most frequent host rocks in the formation of the Şenkaya chrysoprase geologically, and formation was facilitated by the hot meteoric aqueous physico-chemical alteration of nickel-rich ultramafic-ultrabasic rocks. High oxygen isotope ratios indicate that the chrysoprase deposited from mixed solution of meteoric at pneumo-hydrothermal conditions (Skrzypek et al., 2003a and 2003b).

In addition, the $\delta^{18}O_{V\text{-}SMOW}$ based paleo-thermometric temperature of the chrysoprase samples with gemstone quality in the study area is in the range of 60–130 °C while the mean paleo-thermometric temperature is around 96–99 °C. This fact shows that during the deposition of chrysoprase, the $\delta^{18}O_{V\text{-}SMOW}$ value of the water should be taken into consideration in the estimation of the paleo-thermometric state of the ambient. Chrysoprase was precipitated from a very large silicic acid solution rich in trace elements in a mixed meteoric pneumo-hydrothermal environment. However, it should be noted that these values are qualitative (comparative) rather than quantitative (precisely measurable).

Serpentinization and magnesite formation occur as a result of hydrothermal alteration of the peridotites. Therefore, it is seen that peridotites, which have low $SiO_2$ ratio, have high silica ratio and medium and high silica ratios of intermediate samples, there is a hydrothermal diffusion with a high silica ratio in the region and the alteration has developed accordingly. These rocks have experienced various degrees of weathering and chemical alteration (see loss on ignition (LOI) in Table 1). As a result of the field studies, the systematic sampling (Figure 5; Tables 1 and 2) shows that this alteration is in the west-southwest direction, where dacidic volcanism is intense (Narman/Erzurum Volcanite: olivine-augite basalt and augite andesite). In addition, the tectonic thrust direction in the zone where chrysoprase is formed increases the quality of this gemstone.

The abundance of fluid-mobile elements such as Cs, As, and Ba in the samples is due to the addition of the serpentinites with protolith to the mantle rocks during seafloor alteration (Tenthorey and Hermann, 2004). On the other hand, high Ni values indicate that siliceous solutions dissolve some of the nickel found in the serpentines by tectonism and take it into solution. Some of the elements such as Fe, Cr and Ni are definitely responsible for coloring as external lattice defects. However, nickel is the main ion responsible for producing the dark green color (Nagase et al., 1997; Sachanbinski et al., 2001; Witkowski and Zabinski, 2004; Befi, 2009; Shigley et al., 2009; Graetsch, 2011). In addition, almost all samples contain low Au (0.01–0.01 ppm) and Ag (0.01–0.38 ppm), which indicates a wash out in the system. Again, in some samples, "As values" higher than normal are also noteworthy, strengthening this idea (Table 2).

Rare earth element contents normalized to CI chondrite given by McDonough and Sun (1995) are almost close to chondritic values (Figure 11). Most of the samples show an almost flat pattern with a more or less pronounced enrichment in LREE compared to HREE. Although there is no significant anomaly between the

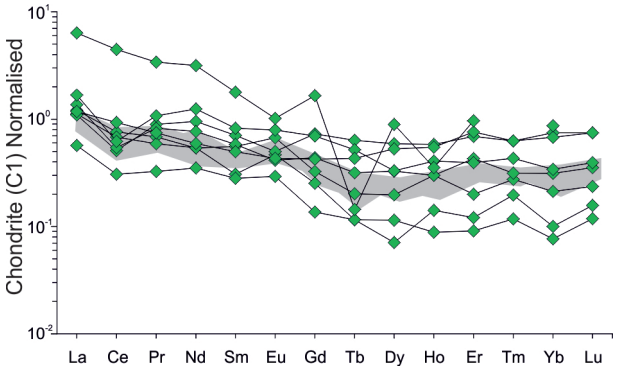


**Figure 11.** Chondrite-normalized REE distribution patterns of chrysoprase samples. The shaded area is shown the host rock samples (host rock data from Şahin (2017)).

elements, there is a depletion of cerium compared to lanthanum. The distribution of REEs provides important information about fluid evolution during hydrothermal circulation in rocks (Elderfield et al., 1988; Haas et al., 1995). However, in many samples slight enrichment of Eu relative to other REEs probably occurred during the interaction between hydrothermal fluids and ultramafic rocks. When chrysoprase samples are compared with host rock REE distributions, it can be said that especially LREE contents of the samples are enriched in varying degrees according to HREEs. Most hydrothermal fluids have remarkably uniform chondrite-normalized REE distribution patterns, with enrichment in the light-REEs relative to the heavy-REEs and a positive europium anomaly (Michard and Albarède, 1986). The chondritic REE contents in chrysoprase suggest an enrichment from serpentinites during hydrothermal alteration processes.

As a result of the evaluation of OCLM studies together with the electron microprobe analysis, the mineral chemistry background of the OCLM colors in opals was revealed. According to OCLM studies, it has been observed that the macroscale colors are not of opal origin, and as a result of opal impregnating the country rock during silicification, the existing colors of these minerals or the colors of their secondary minerals are determinant. In this context, all of the red colors are associated with iron oxides and reflected light microscopy (RLM) observations clearly demonstrate this finding. However, the general formation mechanism and deposition conditions of chrysoprase in the fractures, cracks and voids depend on silicic acid ($H_4SiO_4$), pH (alkaline, 8-9) and Eh (e.g., ambient temperature, origin of water (meteoric or magmatic), water-to-rock ratio, colloidal form).

Although the Şenkaya chrysoprase shows some variation according to their properties, the positive high oxygen isotope values, which clearly indicate the presence of meteoric water, are both due to the geological formation positions of this chrysoprase and the silica phases it contains (e.g., chalcedony and moganite). Geologically, the main wall rocks in the formation of Şenkaya chrysoprase are the serpentinite rocks and chrysoprase was facilitated by the hot meteoric hydrous physico-chemical alteration of nickel-rich serpentinite rocks (Kinnunen and Melisa, 1990; Eggleton et al., 2011).

## 7. Conclusion

In this study, the chemical composition of the chrysoprase in Şenkaya/Erzurum was revealed by geological, mineralogical and petrographical studies. Rocks in the study area are divided into two groups as basement units and cover units. The basement units are the Triassic Zümrüt Formation, Örükyayla Mélange with chrysoprase called Şenkaya emerald and Gedikler Ultramafic rocks. Chrysoprase in the study area has been emplaced in the serpentinites and along the serpentine-basalt contact within the ophiolites. The thickness was determined to vary from 1.5 to 2 m. According to mineralogical and petrographic analysis, chrysoprase has a microcrystalline structure and a cryptocrystalline texture. Intense serpentinization is observed in ultramafic rocks where chrysoprase is located. This intense alteration caused major phases such as olivine and pyroxene to lose their original position in almost all samples and transform into chrysotile, antigorite type serpentine group minerals by transforming in the aqueous environment. In addition, massive opal transitions are common (10%–50%) in the zones where these rocks are found. In general, massive opals are surrounded by magnesite. Opaque minerals in the form of chromite and iron oxide yields are quite common in rocks. Secondary silica (85%–90%) formations, which are common in the cracks of serpentinites, are the main component of chalcedony with very fine grained and very homogeneous distribution.

According to the CL properties of chrysoprase, it was determined that the opal in the samples was a late-stage product as a void filler presenting a semieuhedral comb structure, in the form of crack filling and vein-veinlet. In addition, due to solution chemistry of the mineral did not change significantly during its formation or the trace element changes acting as an activator remained at very low values, it did not produce CL colors, it produced very pale or dull blue colors. ICP-MS analysis indicated that cobalt and predominantly nickel ratio was high (green color) and a contrast between Ni and Co values and $SiO_2$ ratios was determined. Additionally, all samples contain low levels of Au and Ag elements. This situation indicates the presence of a washing in the system.

The results of XRF and XRPD showed that some proportions of cristobalite, quartz, tridymite and a small amount of magnesite are encountered. Mass appearance and $SiO_2$ ratio of chrysoprase were found to

be approximately 91%–94%. In addition, the study area experienced a hydrothermal alteration with a high rate of silica. As a result, a quality chrysoprase has been deposited as a result of both hydrothermal alteration and tectonism.

According to the stable isotope analysis results, the $\delta^{18}O_{V\text{-}SMOW}$ based paleo-thermometric temperature of the chrysoprase samples of the Şenkaya (Erzurum) region with gemstone quality is estimated at 60–130 °C. However, the mean ambient temperature is around 96–99 °C. In addition, this material crystallized from a very large silicic acid solution rich in trace elements in a mixed meteoric origin pneumo-hydrothermal environment. However, these values are qualitative, not quantitative. According to the FTIR-Raman analysis performed on selected samples, the rate of chalcedony quartz silica formation phase in the whole material is approximately 80%, and the ratio of moganite and alpha-quartz silica formation phases is approximately 20% in chrysoprase.

The use of lapidary on chrysoprase in the jewelry industry is difficult to process as it is a fragile and highly sensitive gemstone, because 100 g of processed sample can be obtained from approximately 3 kg of stone. Facet cutting and carving have been finished with great care for the first time on this gemstone. Choker, necklace, and ring designs of chrysoprase processed in the workshop were manufactured. As a result, a special and unique necklace design was produced from chrysoprase.

**Acknowledgments**

This study was supported by the Scientific and Technological Research Council of Turkey (TÜBİTAK) (1001 Project numbered 116Y164 from 2017 to 2019). The authors would like to thank to Prof. Dr. Murat Hatipoğlu, Prof. Dr. Mustafa Kumral, Assoc. Prof. Dr. Şenel Özdamar and Prof. Dr. Emin Çiftçi for their contribution in the evaluation process of this study.

## References

Befi R (2009). Australian chrysoprase with dendritic inclusions. Gems & Gemology-GIA 45 (1): 71.

Çiftçi E (2009). Mercurian sphalerite from Akoluk deposit (Ordu, NE Turkey): Hg as a cathodoluminescence activator. Mineralogical Magazine 73 (2): 165–175. doi: 10.1180/minmag.2009.073.2.257

Çiftçi E, Selim HH, Sendir H (2019). Authentic Semi-precious and Precious Gemstones of Turkey: Special Emphasis on the Ones Preferred for Prayer Beads. 14th International Congress for Applied Mineralogy, pp. 183–188.

Clayton RN, Mayeda TK (1963). The use of bromine pentafluoride in the extraction of oxygen from oxides and silicates for isotopic analysis. Geochimica et Cosmochimica Acta 27 (1): 43–52. doi: 10.1016/0016-7037(63)90071-1

Eggleton, RA, Fitz Gerald J, Foster L (2011). Chrysoprase from Gumigil, Queensland, Australian Journal of Earth Sciences 58 (7): 767-776.

Elderfield H, Whitfield M, Burton JD, Bacon MP, Liss PS (1988). The oceanic chemistry of the rare earth elements. Philosophical Transactions of the Royal Society A 325: 105-126.

Gorobets BS, Rogojine AA (2002). Luminescent spectra of minerals. Reference book. All-Russia Scientific Research Institute of Mineral Resources, Moscow/RU: 300p.

Götze J (2000). Cathodoluminescence microscopy and spectroscopy in applied mineralogy (Vol. 485). Technische Universität Bergakademie Freiberg.

Götze J (2002). Potential of cathodoluminescence (CL) microscopy and spectroscopy for the analysis of minerals and materials. Analytical and Bioanalytical Chemistry 374: 703–708. doi: 10.1007/s00216-002-1461-1

Graetsch Heribert A (2011). Microstructure and origin of colour of chrysoprase from Haneti (Tanzania) Neues Jahrbuch für Mineralogie - Abhandlungen 188 (2): 111–117. doi: 10.1127/0077-7757/2011/0187

Haas JR, Shock EL, Sassani DC (1995). Rare earth elements in hydrothermal systems: Estimates of standard partial molal thermodynamic properties of aqueous complexes of the rare earth elements at high pressures and temperatures. Geochim. Geochimica et Cosmochimica Acta 59: 4329-4350.

Hanchar JM, Miller CF (1993). Zircon zonation patterns as revealed by cathodoluminescence and back-scattered electron images: implications for interpretation of complex crustal histories. Chemical Geology 110: 1–13. doi: 10.1016/0009-2541(93)90244-D

Hanchar JM, Rudnick RL (1995). Revealing hidden structures: the application of cathodoluminescence and back-scattered electron imaging to dating zircons from lower crustal xenoliths. Lithos 86: 289–303. doi: 10.1016/0024-4937(95)00022-4

Hatipoğlu M, Babalık H, Chamberlain SC (2010). Gemstone deposits in Turkey. Rocks & Minerals 85 (2): 124–133. doi: 10.1080/10511970903455868

Hatipoğlu M, İlbeyli N, Kibici Y, Güneş A, Yardımcı Y (2016). Comparison of oxygen isotopic compositions of various chrysoprases in Turkey. 7th Geochemistry Symposium 16-18 May, pp. 194–195.

Heaney PJ (1994). Structure and chemistry of the low-pressure silica polymorphs. In: Reviews in Mineralogy, Volume 29, Silica - Physical behavior, geochemistry, and materials applications. Mineralogical Society of America, Washington, D.C.

Heaney PJ, Post JE (1992). The widespread distribution of a novel silica polymorph in microcrystalline quartz varieties. Science (255/5043): 441–443. doi: 10.1126/science.255.5043.441

Kihara K, Matsumoto T, Imamura M (1986). Structural change of orthorhombic-I tridymite with temperature: A study based on second-order thermal-vibrational parameters. Zeitschrift für Kristallographie 177: 27–38.

Kinnunen K, Malisa EJ (1990). Gem-quality chrysoprase from Haneti-Itiso area, Central Tanzania. Bulletin of the Geological Society of Finland 62: 157-166. doi: 10.17741/bgsf/62.2.006

Konak N, Hakyemez Y, Bilgin R, Bilgiç T, Öztürk Z et al. (2001). Geology of northeast Pontides (Oltu-Olur-Şenkaya-Narman-Uzundere-Yusufeli). MTA Report No: 10489 (in Turkish, unpublished).

Konak N, Hakyemez Y (2008). 1:100.000 scale geological map of Turkey. Kars sheet of G48. MTA Report No: 104: 69p (in Turkish).

Lüle-Whipp Ç (2006). Chromium Chalcedony from Turkey and It's possible Archaeological Connections. 4th International Gemological Symposium & GIA Gemological Research Conference, San Diego, California, USA.

Mcdonough WF, Sun SS (1995). The composition of the Earth. Chemical Geology 120 (3-4): 223-253. doi: 10.1016/0009-2541(94)00140-4

Michard A, Albarède F (1986). The REE content of some hydrothermal fluids. Chemical Geology 55: 51-60.

Michel-Lévy A, Munier-Chalmas CPE (1892). Mémoire sur diverses formes affectées par le réseau élémentaire du quartz. Bulletin de Minéralogie (15): 159–190. doi: 10.3406/bulmi.1892.2278.

Nagase T, Akizuki M, Onoda M, Sato M (1997). Chrysoprase from Warrawanda, Western Australia. Neues Jahrbuch fur Mineralogie, Monatshefte 7: 289–300. doi: 10.1127/njmm/1997/1997/289

Nasdala L, Götze J, Gaft M, Hanchar J, Krbetschek M (2004). Luminescence techniques in Earth Sciences. In: Beran A, Libowitzky E (eds) Spectroscopic methods in mineralogy. Eur Mineral Union Notes in Mineralogy, vol 6. Eötvös University, Budapest, pp. 43–91.

Nasdala L, Beyssac O, Schopf JW, Bleisteiner B (2012). Application of Raman-based images in the Earth sciences. In: Zoubir A (ed) Raman imaging—Techniques and applications. Springer Series in Optical Sciences, vol 168. Springer, Berlin, pp. 145–187.

O'Neil JR (1986). Terminology and standards. In: Valley J W, Taylor H P, O'Neil J R (eds.) Stable Isotopes in High Temperature Geological Processes. Mineralogical Society of America, pp. 561-570.

Robertson A, Parlak O, Ustaömer T, Taslı K, İnan N et al. (2013). Subduction, ophiolite genesis and collision history of Tethys adjacent to the Eurasian continental margin: new evidence from the Eastern Pontides, Turkey. Geodinamica Acta 26 (3-4): 230–293. doi: 10.1080/09853111.2013.877240

Sachanbinski M, Janeczek J, Platonov A, Rietmeijer FJM (2001). The origin of color of chrysoprase from Szklary (Poland) and Sarykul Boldy (Kazakhstan). Neues Jahrbuch für Mineralogie–Abhandlungen 177: 61–76. doi: 10.1127/007777502753418584

Schiffries CM, Rye DM (1989). Stable isotopic systematics of the Bushveld Complex: I. Constraints of magmatic processes in layered intrusions. American Journal of Science 289 (7): 841–873. doi: 10.2475/ajs.289.7.841

Selim HH (2015). Turkey's precious and semi-precious gemstones. İTO Journals, 2014 (4), 102p (in Turkish).

Selim HH, Güçtekin A, Kaya M, Taş KÖ, Tanç B et al. (2019a). Determination of economic potential and geochemical, gemological properties of green opal called Şenkaya (Erzurum) emerald. TÜBİTAK 1001 Project No: 116Y164, 137p (in Turkish, unpublished).

Selim HH, Güçtekin A, Şahin F, Güner E, Korkutan E et al. (2019b). Gemological properties of Şenkaya/Erzurum chrysoprase (Emerald) and usage in jewelery sector. 72nd Geological Congress of Turkey with international participation, pp. 117–118.

Schertl HP, Neuser RD, Sobolev NV, Shatsky VS (2004). UHP metamorphic rocks from Dora Maira/Western Alps and Kokchetav/Kazakhstan: New insights using cathodoluminescence petrography. European Journal of Mineralogy 16 (1): 49–57. doi: 10.1127/0935-1221/2004/0016-0049

Shigley JE, Laurs BM, Renfro ND (2009). Chrysoprase and prase opal from Haneti, central Tanzania. Gems & Gemology 45 (4): 271–279.

Skrzypek, G, Jedrysek, MO, Sachanbinski, M (2003a). Oxygen stable isotope geochemistry of chrysoprase from wiry and Szklary Mines (SE Poland). In: Conference papers of International Symposium on Isotope Hydrology and Integrated Water Resources Management, 19–23 May, Vienne, Austria, pp. 470–472.

Skrzypek, G, Sachanbinski, M, Jedrysek, MO (2003b). Oxygen isotope evidence for low temperature formation of chrysoprase. Polskie Towarzystwo Mineralogiczne–Prace Specjalne Mineralogical Society of Poland–Special Papers, Zeszyt 22, pp. 204–206.

Şahin F (2017). Gemological characteristics of green opal. Dissertation, İstanbul Commerce University Graduate School of Applied and Natural Sciences Department of /Jewelery Engineering 119p (in Turkish, unpublished).

Şahin F, Selim HH., Güçtekin A, Taş KÖ, Güner E (2017). Occurrence and use in jewelry sector of green opal named Şenkaya (Erzurum) emerald. 70th Geological Congress of Turkey, pp. 138–139.

Tenthorey E, Hermann J (2004). Composition of fluids during serpentinite breakdown in subduction zones: Evidence for limited boron mobility. Geology 32 (10): 865–868. doi: 10.1130/G20610.1

Vıcıl M, Çavuşoğlu İ, Celep O, Alp İ, Yılmaz AO (2004). Opal and general properties. 5th Symposium on Industrial Raw Materials, Dokuz Eylül University Engineering Faculty Mining Engineering Department, 329p (in Turkish).

Witkowski S, Zabinski W (2004). Application of the TPR method for the studies of Ni (II) in chrysoprase. Journal of Thermal Analysis and Calorimetry 77 (1): 143–148. doi: 10.1023/b:jtan.0000033197.08164.ab

Zaimoğlu Ö, Kaplanoğlu M (2012). Oltu Emerald in Jewelry. Batman University Journal of Life Sciences 1 (1): 1101–1116 (in Turkish).